A new repository of electrical resistivity tomography and ground penetrating radar data from summer 2022 near Ny-Ålesund, Svalbard

Francesca Pace[1], Andrea Vergnano[2], Alberto Godio[1], Gerardo Romano[3], Luigi Capozzoli[4], Ilaria Baneschi[5], Marco Doveri[6], Alessandro Santilano[7]

[1] Department of Environment, Land and Infrastructure Engineering (DIATI), Politecnico di Torino, Turin, 10129, Italy.
[2] Department of Earth Sciences (DST), Università degli Studi di Torino, Turin, 10125, Italy.
[3] Dipartimento di Scienze della Terra e Geoambientali, Università degli Studi di Bari Aldo Moro, Bari, 70125, Italy.
[4] Institute of Methodologies for Environmental Analysis, National Research Council (CNR), Tito, 85050, Italy
[5] Geosciences and Earth Resources (IGG) - National Research Council of Italy (CNR), Pisa, 56124, Italy
[6] Dipartimento di Scienze della Terra, Pisa University, Pisa, 56126, Italy.
[7] Geosciences and Earth Resources (IGG) - National Research Council of Italy (CNR), Messina, 98166, Italy

Correspondence to: Francesca Pace (francesca.pace@polito.it)

Abstract.

We present the geophysical data set acquired in the summer of 2022 close to Ny-Ålesund (Western Svalbard, Brøggerhalvøya peninsula - Norway) as part of the project ICEtoFLUX. The aim of the investigation is to characterize the role of groundwater flow in correspondence of the active layer as well as through and/or below the permafrost. The data set is composed of Electrical Resistivity Tomography (ERT) and Ground Penetrating Radar (GPR) surveys, which are well-known geophysical techniques for the characterization of glacial and hydrological processes and features. 18 ERT profiles and 10 GPR lines were acquired, for a total surveyed length of 9.3 km. The data have been organized in a consistent repository that includes both raw and processed (filtered) data. Some representative examples of 2D models of the subsurface are provided, that is, 2D sections of electrical resistivity (from ERT) and 2D radargrams (from GPR). These examples can support the identification of the active layer. The data set is of major relevance because there is little geophysical data published about the Ny-Ålesund area. Moreover, these geophysical data can foster multidisciplinary scientific collaborations in the fields of hydrology, glaciology, climate, geology, geomorphology, etc. The geophysical data are provided in a free repository and can be accessed at the repository under data doi (Pace et al., 2023, https://zenodo.org/doi/10.5281/zenodo.10260056).

1 Introduction

The Earth's interior and its physical properties are imaged by quantitative methods. Geophysical measurements on the Earth's surface can reveal how the subsurface physical properties vary in space, and possibly in time.

The Svalbard Archipelago (High Arctic Norway, see Fig. 1a) is believed to be a representative typical Arctic critical environment (Dallmann, 2015). The location of the Svalbard Archipelago is ideal for observing the Arctic environment in
35   general, from the perspectives of glaciology, geology, biodiversity, and impact of climate change (Gevers et al., 2023). Climate change heavily affects the Arctic hydrologic dynamics, generating significant environmental modifications and potentially leading to the climatic feedback and warming amplification (Wadhams, 2017).

Ny-Ålesund is the northernmost settlement in the world (79° North), located in western Spitsbergen in the Svalbard Archipelago (see Fig. 1b). It serves as a scientific hub for the international research community and its logistical support
40   (Paglia, 2020). Ny-Ålesund represents an outstanding natural lab for any topics of scientific research in the Arctic, being situated in the Kongsfjorden fjord, where glaciers, rivers, coast, sea, atmosphere, animals, plants and their interaction can be monitored (Gevers et al., 2023; Pedersen et al., 2022). From a geophysical standpoint, the Svalbard Archipelago is interesting because of the presence of permafrost, seasonal active layer, springs, aquifers, sea water and old coal mines. Spatial heterogeneity in geophysical properties is expected due to the local lithology and structural framework as well as the
45   geomorphologic features linked to the past movement of the glaciers (Orvin, 1934; Dallmann, 2015).

Geophysical techniques, such as Electrical Resistivity Tomography (ERT) and Ground Penetrating Radar (GPR), have been used to survey Arctic areas all around the world, for example to detect heterogeneity in the permafrost, to monitor glacial and periglacial processes or to understand the role of ice in the hydrology (Hauck and Kneisel, 2008; Rossi et al., 2022). The ERT method has been successfully adopted in the Arctic environment because of its effectiveness in imaging the variation in
50   the electrical resistivity values of aquifers, permafrost, and active layer. They can be easily distinguished by their difference in the resistivity value: high for the permafrost and low for the water-saturated soil. The GPR method is largely adopted for glaciological studies because the radar signal travels easily and with little attenuation in pure ice, reaching hundreds of meters in ideal conditions. Moreover, the GPR signal, whose traveling time and impedance are based on the dielectric permittivity of the material, can clearly distinguish frozen and non-frozen conditions, because ice and water have different
55   values of dielectric permittivity.

The permafrost has been mainly investigated by GPR and ERT, to test monitoring systems for its temporal variations (Westermann et al., 2010), its physical properties (Schwamborn et al., 2005), the properties of the patterned ground typical of permafrost areas (Park et al., 2023), its water content with Time Domain Reflectometry (Lee et al., 2018), its impacts to quarry activities (Koster and Kruse, 2016), and landslide phenomena (Kuschel et al., 2019). In glacier research, the local
60   polythermal glaciers of the Kongsfjorden peninsula were studied, mainly with the GPR technique, to investigate the cold-temperate transition surfaces (Schannwell et al., 2014), ice thickness (Saintenoy et al., 2011), snow-firn properties (Kohler et al., 2003), buried ice (Soldovieri et al., 2009), glacier dynamics and hydrology (Tolle et al., 2011).

Ny-Ålesund is an ideal place for also hydrogeological studies, because 3 km away from the settlement there is the Bayelva River catchment, where the entire water cycle from the glaciers to the sea can be studied within an area of a few squared
65   kilometers (see Fig.1). Applied geophysics can be of great help to unravel the complexity of the water cycle and to improve knowledge about groundwater flow by means of non-destructive measurements from the surface. In formerly glacierized

watersheds, hydrologic processes are evolving, with new storage mechanisms and distribution of water resources, such as more persistent rivers and developed groundwater systems. Over the past years, investigations on the Arctic freshwater increased but wide knowledge about processes that govern water flow dynamics in High Arctic basins is still quite limited

70 (Svendsen et al., 2002). The Bayelva catchment has been largely investigated from a glaciological standpoint (Boike et al., 2018), but there are sporadic studies on its freshwater (Doveri et al., 2019; Repp, 1988; Haldorsen and Heim, 1999; Killingtveit et al., 2003).

The ICEtoFLUX (I2F) project has been funded by the Italian Plan for Research in the Arctic and stands for HydrologIcal changes in ArctiC Environments and water-driven biogeochemical FLUXes (https://www.icetoflux.eu/). I2F focuses on the

75 hydrologic dynamics and related effects in the Bayelva River catchment, from its glaciers and proglacial system down to the Kongsfjorden fjord sector affected by the river. Experimental activities on hydrology, geo- and environmental chemistry, microbiology and geophysics, and numerical modelling, all concerning water cycle components, were planned and carried out to quantify hydrologic processes and related biotic-abiotic transports. Four piezometers were drilled and monitored in the frame of the I2F project to be used as benchmark for the geophysical study.

80 We carried out an integrated geophysical survey in the proglacial zone of the glaciers Vestre and Austre Brøggerbreen close to the Ny-Ålesund settlement (Fig. 1c). The geophysical techniques adopted were ERT and GPR due to their well-established advantages in the Arctic environment, and Magnetotelluric (MT) for its high investigation depth (from hundreds of meters to tens of kilometers). The objective of the geophysical survey relies on the study of the presence and role of groundwater flow in correspondence of the active layer as well as through and below the permafrost. A specific target is

85 represented by the possible groundwater flow at the basis or through the permafrost and the circulation at a depth where the ground is supposed to be permanently frozen. This study is also aimed to support the multidisciplinary study about the interactions between superficial water, groundwater circulating in the active layer and deep aquifer.

This paper presents the collection of geophysical data acquired in summer 2022 as part of the I2F project. The objective of this paper is to make available the data set to the scientific community and hence foster advances, interpretations and

90 collaborations with and among the stakeholders. The data here presented are intended to provide a major contribution to research because there have been few studies that have published geophysical data from the Ny-Ålesund area so far.

This paper begins by introducing the study area where the geophysical data were acquired. Then, it describes the geophysical survey, the acquisition configurations, and the challenges encountered in the remote Arctic environment. Another section is concerned with the raw data set and the processed data after quality control. Then, some representative geophysical models

95 are presented. Finally, the organization of the repository and of the data files are carefully described.

2 Study area

The study area is located on the South-Western coast of the Kongsfjorden at 78°55' northern latitude in correspondence of Ny-Ålesund. The Ny-Ålesund settlement is a polar scientific outpost on the Brøggerhalvøya peninsula that is surrounded by

tundra and glaciers (Brøggerbreen and Lovénbreen) on one side and faces the Fjord Kongsfjorden on the other side. Mt.

100 Zeppelin stands out in the area (see Fig. 1c).

The history of this Arctic region is necessarily tied together with the geoscientific exploration by pioneers driven by the thirst for knowledge or by the urge to run the (black) gold rush being this land rich in coal deposits (Dallmann, 2015). The geology of this has been accurately investigated since the beginning of the 20th century with a particular focus on the coal ore deposits that were exploited until 1962 (Hoel, 1925; Orvin, 1934).

105 The Svalbard Islands are located on the north-western corner of the Eurasian plate (Horota et al., 2023). The outcropping rocks in the Archipelago represent a natural geological archive of the Earth' evolution since its early history, from Archean to recent times. Major tectonic events affected the bedrock of Svalbard Islands including the Caledonian orogeny, which resulted in the deformation of the Pre-Devonian metamorphic and sedimentary basement. Svalbard's sedimentary succession from Devonian-to Paleogene is nearly complete and comprises a wide range of lithologies (conglomerates, sandstones,

110 shales, carbonates, and evaporites). The main rock types are dated from Carboniferous and Permian (limestones and dolomites) to Tertiary sandstones (Fig. 2). Widespread moraines deposits occur in the study area.

The area hosted the northernmost productive coal field in the world. The coal-seams are of Tertiary age, Paleocene or Eocene (Hoel, 1925). The strata briefly consist of sandstones, with subordinate layers of conglomerates, shales, and coal. The coal-seams are concentrated in the lower and upper parts of the Triassic sedimentary sequence (Orvin, 1934). In the

115 lower coal horizon, the most important seams are (from down to top) the Ester, Sofie and Advokat seams. The Agnes-Otelie, Josefine, and Ragnhild seams are on the upper horizon.

The surroundings of Ny-Ålesund have been previously investigated by means of ERT surveys for glacier and landslide monitoring (Lee et al., 2018; Park et al., 2023; Kuschel et al., 2019) and GPR surveys for glaciological studies (Schwamborn et al., 2005, 2008; Westermann et al., 2010; Saintenoy et al., 2011, 2013; Kumari et al., 2021). Several geophysical studies

120 involved other regions far from Ny-Ålesund: the Kongsfjorden fjord (Lindbäck et al., 2018), central Spitsbergen(Beka et al., 2017; Keating et al., 2018; Hornum et al., 2021) and south-western Spitsbergen (Kasprzak et al., 2017).

The Research in Svalbard Portal provides the list of the past and present projects carried out around Ny-Ålesund and adopting geophysical techniques. A non-exhaustive list is composed of the projects PRISM (Kuschel et al., 2019), SEISMOGLAC and CalvingSEIS (Köhler et al., 2015), GRAVITE (Mémin et al., 2014), among the others. Other non-

125 geophysical studies involving the surroundings of Ny-Ålesund included borehole investigations (Boike et al., 2018; Gevers et al., 2023), geotechnical surveys (Byun et al., 2014), numerical modeling (Booij et al., 1998; Boike et al., 2003; Pramanik et al., 2018) and other complementary measurements of the soil or groundwater (Tolle et al., 2011; Doveri et al., 2019; Son and Lee, 2022).
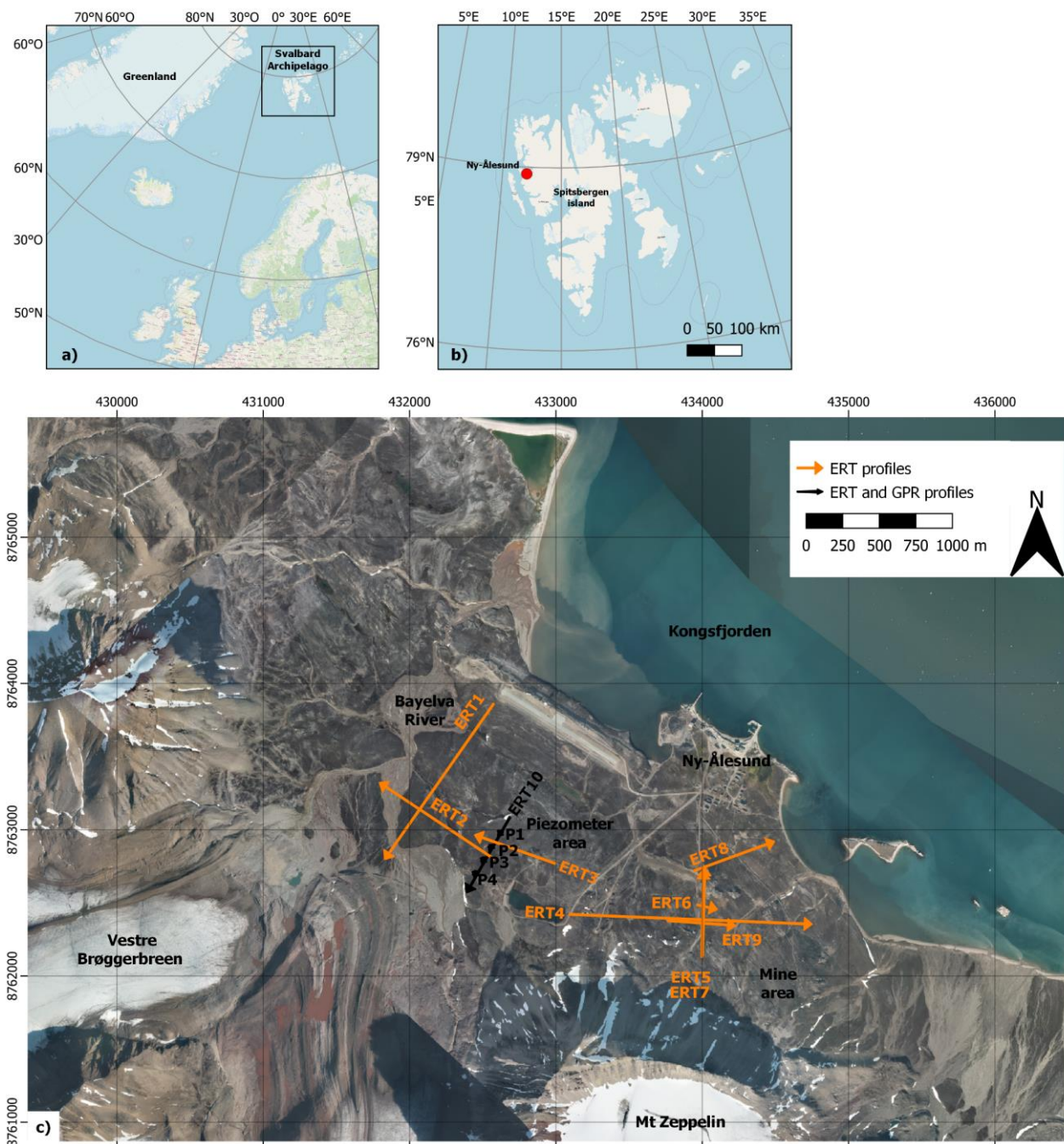
Figure 1: a) location of the Svalbard Archipelago; b) location of Ny-Ålesund on Spitsbergen, western Svalbard; c) a general overview of the area investigated by the ICEtoFLUX project. The Ny-Ålesund settlement is close to the catchment of the Bayelva River. The orange lines represent the ERT profiles (from ERT1 to ERT10 and P1-P4). The black lines represent the profiles where both ERT and GPR were acquired. The coordinate system is WGS84-UTM33N. The satellite picture in background was exported from the WebGIS tool by ©Norwegian Polar Institute (https://geokart.npolar.no/Html5Viewer/index.html?viewer=Svalbardkartet

135   ). **Some of the acquisitions overlap fully or partially: two surveys were performed in July-August 2022 and in August-September 2022, to possibly find some variations over time.**
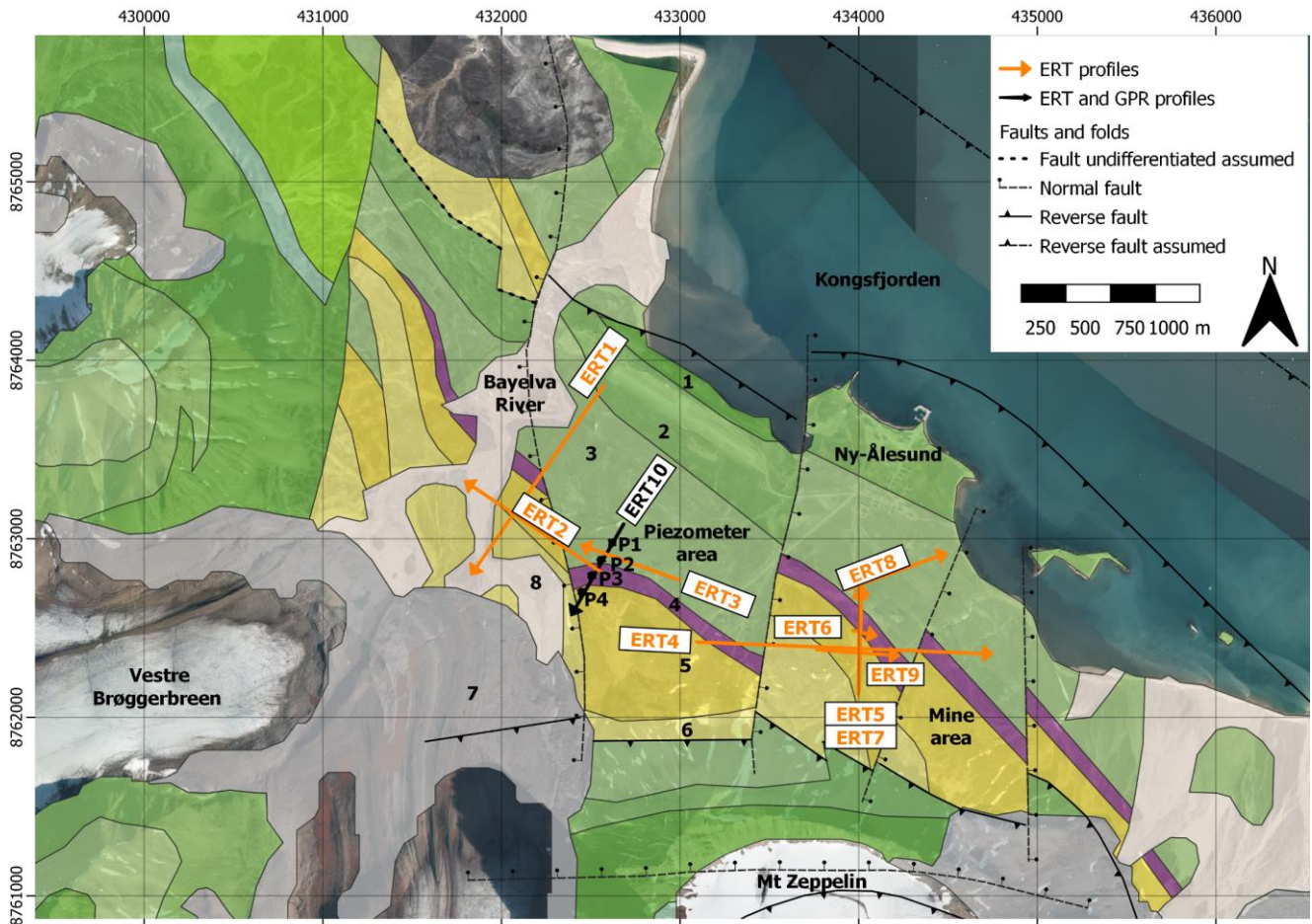
Figure 2: Geological map (data from NPI, WMS geological map at 1:250.000): 1) Carbonate rocks of Wordiekammen Formation (Moscovian-Sakmarian)); 2) Carbonate rocks of Gipshuken Formation (Sakmarian - Artinskian); 3) Chert, shale, sandstone and
140   **limestone of Kapp Starostin Formation (late Artinskian - Late Permian); 4) Shale, siltstone, sandstone of Vardebukta Formation (Induan); 5) Sandstone, shale, coal of Kongsfjorden Formation (paleocene ?); 6) Sandstone, shale, conglomerate of Brøggerbreen Formation (Paleocene?); 7) Moraine (Holocene); 8) Glacio-fluvial deposits (Holocene); NF) Normal fault; RF) Reverse fault. The coordinate system is WGS84-UTM33N. The geological map was exported from the WebGIS tool by ©Norwegian Polar Institute (https://geokart.npolar.no/Html5Viewer/index.html?viewer=Svalbardkartet).**

145   ## 3 The geophysical survey

3.1 ERT and GPR methods

ERT is an active geophysical technique that involves the injection of current into the subsoil, and the measurement of the consequent voltage distribution at the surface. The current is injected in a dipole of electrodes, called transmitter or source, while the voltage is measured at one or multiple dipoles, called receiver(s). The measured voltage is influenced by the

150 current flowing in the subsoil, which is, in turn, dependent on rock types, porosity, water saturation, salinity and temperature, weathering, metallic content, and clay content. The transmitter and the receivers can be placed in several relative positions or configurations. Different configurations are sensitive to different patterns of resistivity distribution. In the Ny-Ålesund survey, mainly three configurations were employed: Wenner (WE), Wenner-Schlumberger (WS) and Dipole-Dipole (DD). While WE and WS are sensitive to the vertical layering of the subsoil, DD is sensitive to lateral resistivity contrasts

155 (Martorana et al., 2017).

GPR is a non-invasive methodology that detects electromagnetic (EM) impedance contrasts in a medium. It is based on the analysis of the reflections of electromagnetic waves transmitted into the ground depending on the frequency of the electromagnetic waves and the electrical characteristics of the potential targets and surrounding soil (electrical permittivity and conductivity). The use of different antennas and frequencies enables the imaging of subsoil at different penetration

160 depths: the lower the frequency the larger the penetration. Therefore, the operating frequency is always a trade-off between resolution and penetration depth. In our survey, GPR was planned to retrieve high-resolution information at a relatively shallow depth. Two different antennas were adopted with different frequencies: 400 MHz and 40 MHz. The emitted signal at the high frequency (400 MHz) allows detailed information up to four meters of depth to be obtained, that is enough to image the expected interface between the active layer and the permafrost. The 40-MHz signal was planned to reach 10-20 m of

165 depth (Jol, 2009)

3.2 MT method

The MT method is a natural-source electromagnetic method that measures the Earth's response to the low-frequency EM waves coming from the magnetosphere and ionosphere. The measurement of the electrical and magnetic fields allows determining the electrical resistivity of the Earth at depths ranging from some meters to hundreds of kilometers (Chave et al.,

170 2012). The acquisition of MT data is performed with no transmitters since the signal has a natural origin. Two components (horizontal and perpendicular) of the electric field and three components of the magnetic field are measured on the ground surface.

An MT survey was planned in the Bayelva area as part of the I2F project, but a first attempt had with no success. Two systems were adopted for Audio-MT and Broad-Band MT acquisition. The planned MT survey had to be stopped after the

175 acquisition of 5 soundings due to an unexpected high level of anthropic electromagnetic noise.

The MT data would have been useful for the deep characterization of the permafrost and potential sub-permafrost aquifer. However, the MT data processing performed after the first acquisition revealed a wide-band and energetic noise source whose presence prevented the possibility of acquiring good-quality MT data. This was completely unexpected because Ny-Ålesund is a radio silent and geographically remote settlement, where wireless equipment is not allowed to ensure a high

180 signal-to-noise ratio for the data measured. This restriction is probably duly working for very high frequency signals (in the order of giga Hz). The most corrupted MT signals were in the frequency bands > 1Hz. The presence of this kind of noise in the recorded MT time series resulted in the impossibility of obtaining reliable MT estimates.

The MT survey was shut down, but our experiment can be of help for future geophysical expeditions in Ny-Ålesund.

3.3 Data acquisition

185   Three different sectors around Ny-Ålesund were surveyed (Fig. 2): i) the Bayelva catchment on the west, ii) the piezometer area close to the Amundsen-Nobile climate change tower (CCT), and iii) the mine area on the east (close to the Ester spring). The ERT survey was divided into two campaigns in July and September 2022. The instrument was the georesistivimeter Syscal Pro (Iris instruments). The receiver was multichannel with a maximum of 10 measurements at a time and a maximum number of 48 electrodes for each acquisition. The configurations of the acquisition were DD, WS and WE. The acquisition

190   was usually moved forward by using the roll-along technique. The acquisition settings of the instruments were an injection time of 500 ms and a number of minimum 3 up to 6 stacks. The accepted error percentage on the stacks was 2%. A total length of 7.87 km was acquired along 18 profiles (Fig. 1c and Table 1). The electrode spacing was 10 m for 9 profiles (deep ERTs), 1 m for 8 profiles and 2 m for the remaining one (shallow ERTs). The details about the acquired ERT profiles are schematized in Table 1.

195   **Table 1: Data acquisition parameters and array configuration for ERT profiles. The coordinate system is WGS84-UTM33N.**

Name	Length (m)	Spacing (m)	Arrays	Roll Along	East – 1st electrode	North – 1st electrode	East – last electrode	North – last electrode
ERT1	1310	10	DD, WS	7	432575	8763862	431830	8762798
ERT2	950	10	DD, WS	4	432577	8762801	431794	8763323
ERT3	590	10	DD, WS	1	432997	8762768	432446	8762965
ERT4	1670	10	DD, WS	10	433091	8762422	434750	8762355
ERT5	590	10	DD, WS	1	433998	8762128	434009	8762718
ERT6	142	2	DD, WS	2	433965	8762488	434102	8762456
ERT7	590	10	WE, WS, DD	1	433997	8762124	434012	8762710
ERT8	590	10	WE, WS, DD	1	433936	8762703	434483	8762899
ERT9	470	10	WE, WS, DD	0	433763	8762384	434227	8762341
ERT10	590	10	WE, WS, DD	1	432674	8763075	432383	8762567
ERT_P1_Ort	47	1	WS	0	432602	8762986	432637	8762962
ERT_P1_Par	47	1	WS	0	432625	8762993	432602	8762952
ERT_P2_Ort	47	1	WS	0	432536	8762881	432580	8762871
ERT_P2_Par	47	1	WS	0	432563	8762896	432542	8762854
ERT_P3_Ort	47	1	WS	0	432486	8762800	432526	8762775
ERT_P3_Par	47	1	WS	0	432516	8762806	432491	8762767
ERT_P4_Ort	47	1	WS	0	432429	8762708	432470	8762683

| ERT_P4_Par | 47 | 1 | WS | 0 | 432460 | 8762715 | 432437 | 8762675 |

The two 10m-spacing profiles in the Bayelva catchment (ERT1 and ERT2) are perpendicular and very close to the Bayelva River, that is crossed at the end of the two ERTs toward the glaciers. In the area of the piezometers, there are two perpendicular 10m-spacing profiles (ERT3 and ERT10) and 8 short profiles (1m-spacing) that cross the four piezometers (P1, P2, P3, P4) in parallel and orthogonally. Then, the mine area is crossed by the longest line ERT4 (1.67 km), which

200   partially overlaps ERT9. Three profiles cross the Easter spring (ERT5, ERT6, ERT7) and a profile is directed towards the sea (ERT8). ERT7 and ERT5 are partially coincident because they were measured during two different campaigns, in July and September 2022, respectively. The same applies to ERT9 and ERT4, respectively. The ERT6 was acquired with 2m-spacing.

The GPR survey was carried out in the piezometer area, as shown in Fig. 2. The cumulative surveyed length is about 1400

205   meters along 10 GPR lines. Each line has been measured in a direct and reverse sense for a total surveyed length of 2800 meters. The 400 MHz antenna was used to measure GPR radargrams along the 8 shallow ERT profiles centered in the four piezometers (P1, P2, P3, P4) and along the ERT10 line crossing all the piezometers. The antenna at 40 MHz was adopted for a line in correspondence of the ERT10. The details about the acquired GPR profiles are schematized in Table 2.

The GPR data were acquired with the GSSI SIR-3000 GPR System coupled with two different antennae working at the

210   frequencies of 40 and 400 MHz. The adopted recording time window is set to 120 ns for the acquisition performed with the 400 MHz antenna and 1200 ns for the data acquired with the 40 MHz antenna. Data acquired were discretized by 512 time-samples. The acquisitions were carried out without a survey wheel and to assign the right coordinates to each recorded trace, several marks were placed every 5 meters.

Table 2: Data acquisition parameters for GPR profiles.

Name	Length (m)	Frequency (MHz)	East – starting profile	North – starting profile	East – ending profile	North – ending profile
GPR_P1_Ort	50	400	432602	8762986	432638	8762960
GPR_P1_Par	50	400	432625	8762993	432600	8762950
GPR_P2_Ort	50	400	432536	8762881	432583	8762870
GPR_P2_Par	50	400	432563	8762896	432539	8762851
GPR_P3_Ort	50	400	432486	8762800	432529	8762773
GPR_P3_Par	50	400	432516	8762806	432489	8762764
GPR_P4_Ort	30	400	432429	8762708	432455	8762692
GPR_P4_Par	28	400	432460	8762715	432446	8762690
GPR_Long_40MHz	590	40	432674	8763075	432383	8762567
GPR_Long_400MHz	445	400	432447	8762693	432642	8763023

4 The data set

4.1 Raw data and quality control

As standard, each ERT data acquisition was preceded by the check of the contact resistance between the electrodes and the ground. This operation ("RS check") was directly performed by the instrument. As an additional quality control (QC), specific electrodes (occupying a known position along the geoelectrical lines) were unplugged before starting the contact resistance check in order to verify the correct number addresses of the electrodes. When one of the unplugged electrodes was involved in the RS check, the georesistivimeter stopped the check operation as long as the electrodes were correctly plugged. For some of the profiles (ERT7, 8, 9,10 and ERT_P1, P2, P3, P4), the contact resistance values were stored together with the WS geoelectrical data to enhance a posteriori control of the data quality and monitoring of the measuring conditions.

At the end of each ERT survey, an in-field evaluation of the collected data quality was performed. Data were downloaded from the georesistivimeter and visualized as pseudosections of apparent resistivity (Fig. 3). The regularity of the data distribution in relation to the measuring conditions was used to drive decision-making on the necessity of repeating data acquisition or change investigation strategy.

Noisy data in the geoelectrical measurements can be due to soil conditions, complex subsoil structures or instrumental failure. Soil conditions can negatively affect the ERT data if the ground-electrode electrical contact is not ideal. This condition is common in those areas where stones and gravels cover the ground surface, such as in the Bayelva catchment and in the mine area. Bentonite was used to improve the ground-electrode contact when necessary.

The QC on the field for the GPR data was aimed to verify the proper functioning of the GPR acquisition system (control unit + antennas) and the correct settings of the acquisition parameters (time window, sampling rate, gain, trace increment, etc.). The QC was preliminarily done, during the data acquisition process, directly on the GPR acquisition system monitor. Subsequently, a more thorough verification was performed in the lab after the acquisition, resulting in the elaboration of preliminary 2D radargrams.

4.2 Processed data

The ERT data were pre-processed by using the software Prosys-III (Iris instruments). The filtering procedure of ERT data was based on the verification of some general criteria. For each geoelectrical profile the preprocessing consisted of discarding the following data:

- negative resistivity values,
- electrodes with anomalous values of contact resistance ("RS check"),
- isolated extremely high or low resistivity values (i.e., outliers).

An example of ERT data, i.e., a pseudo-section of apparent resistivity, measured along the ERT_P1_Par with a WS configuration is depicted in Fig. 3. The ERT_P1_Par profile is centered at the piezometer P1 and is parallel to ERT10. This profile was chosen as representative since GPR data were acquired at the same location (see section 5.2). The whole set of

pseudo-sections measured along each ERT is presented in the repository (see Section 6 for details). The filtered ERT data were then ready to be inverted to create 2D geoelectrical models of the subsoil (see Section 5.1).
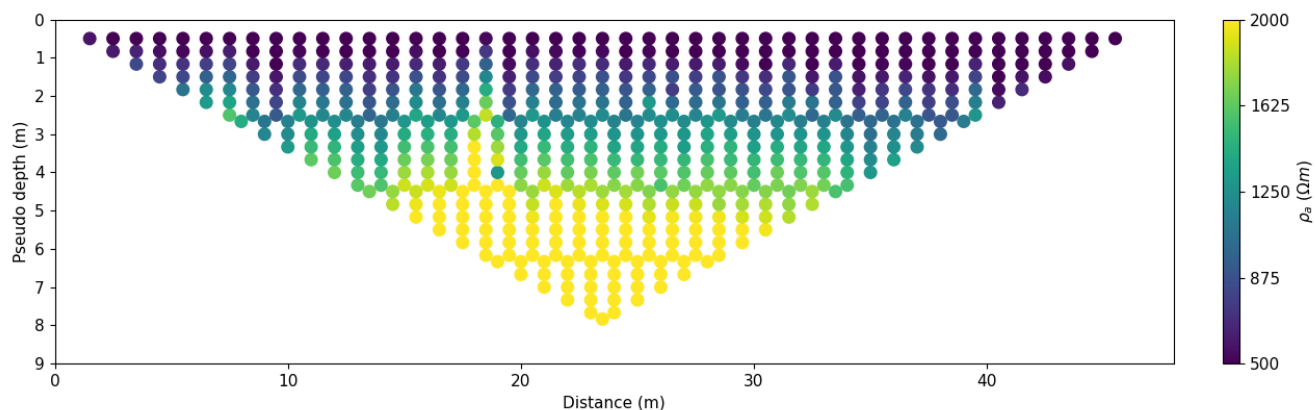
Figure 3: Example of experimental pseudo section of the ERT_P1_Par profile showing the spatial distribution of the measured apparent resistivity (ρ_a) values (in Ωm). The acquisition configuration is WS.

The GPR data were processed with Reflexw software (Sandmeier, 2021), according to the following processing steps:

- The distance between each trace was set in order to match, every 5 meters, the geolocation of the marker, with the "marker interpol." processing step.

- A time-zero correction was performed, with the "move startime" processing step, by manually selecting, as time zero, the value in nanoseconds correspondent to the beginning of the transmitted impulse.

- A background removal filter was applied over the whole profile, subtracting the average trace from each trace.

- A subtract-mean, or "dewow" filter was used with a time window of 2 ns, to remove possible instrumental voltage shift in the data.

- A manually selected gain function, based on subjective choice and experience, was applied to contrast the effects of signal attenuation and geometric dispersion.

- A bandpass filter removed the frequencies under about 150 MHz and above about 550 MHz.

The data processing chain is shown in Fig. 4.

For visualization, the topographic correction of the data was performed by using the topographic surface retrieved from a recent Digital Elevation Model with 5 meters of resolution, published by the Norwegian Polar Data Centre and available as basemap data "Svalbard digital elevation models" at https://geodata.npolar.no (©Norwegian Polar Institute, 2014). Each radargram was normalized to its amplitude mean value.
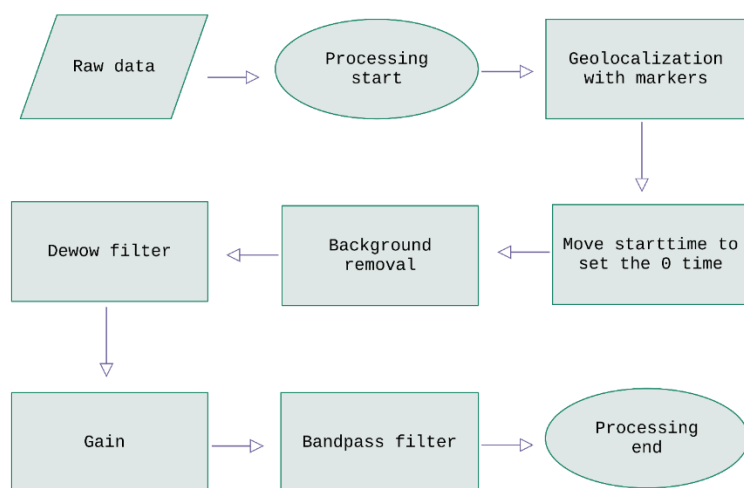
Figure 4: GPR processing chain adopted for the GPR lines of the ICEtoFLUX project.

5 Representative results

5.1 ERT inversion method

The ERT data pre-processing and filtering of the outliers is followed by the geophysical inversion of the acquired data. The inversion aims at finding the best resistivity distribution of an earth model which explains the data within a certain error threshold.

The 2D ERT inversion was performed by using the open-source package ResIPy (Blanchy et al., 2020). ResIPy can be used for geoelectrical data (direct-current and induced polarization measurements) and provides several tools such as high-level filtering, error modelling, inversion/forward modelling and post-processing. It can be accessed from a Python application programming interface (API) or a standalone graphical user interface (GUI). Further information about ResIPy and other software for electrical resistivity modelling can be found in Doyoro et al. (2022) and Loke et al. (2013).

In the inversion process, the same subsoil discretization was adopted in terms of cell growing factor, characteristic length, and background resistivity. The boundary depth was 80 m for the ERT lines with 10 m of spacing between electrodes. The cell growth factor was 0.7. The characteristic length was kept as the ResIPy default to ensure two nodes between two consecutive electrodes. The topography was included. The inversion type was a regularized inversion with linear filtering and normal regularization. The same inversion settings were adopted for all the quadrupole configurations (WE, WS, DD).

The only exception was for the measurement errors given to the inversion. For the WE and WS data sets, the data error was set to 2%, in agreement with the largest observed staking errors. For the DD data sets, an ad hoc error model (linear or power law) was calculated from reciprocal error distribution and used in the inversion procedure.

The number of iterations was between 2 (for short profiles) and 10 (e.g., for the longest ERT4), and they were computed in few seconds. The final root-mean-square errors (RMSEs) ranged between 1 (the minimum threshold to end the inversion) and 2.18 (for ERT4, which had high errors).

5.2 ERT models

The inversion result for the ERT_P1_Par (WS configuration, 1 m of spacing) is presented in Fig. 5. The resistivity model shows a gradual increase in resistivity with depth. At shallow depth, up to 2 m of depth b.g.l., the resistivity range is 100 – 500 Ωm, while from 2 m of depth down to the bottom of the model the resistivity rises to 1000 Ωm and even up to 8000 Ωm, which can be theoretically correlated with permafrost. The interpretation of the resistivity model goes beyond the scope of this paper and needs multidisciplinary insights, given that the resistivity of the frozen rock might be site-specific. To the best of the authors' knowledge there is no direct measurement of electric resistivity in the investigated area, except for few and old superficial electric-conductivity sensors installed up to 1 meter of depth in the Bayelva basin (KODAMA et al., 1995; Boike et al., 2018; Son and Lee, 2022).
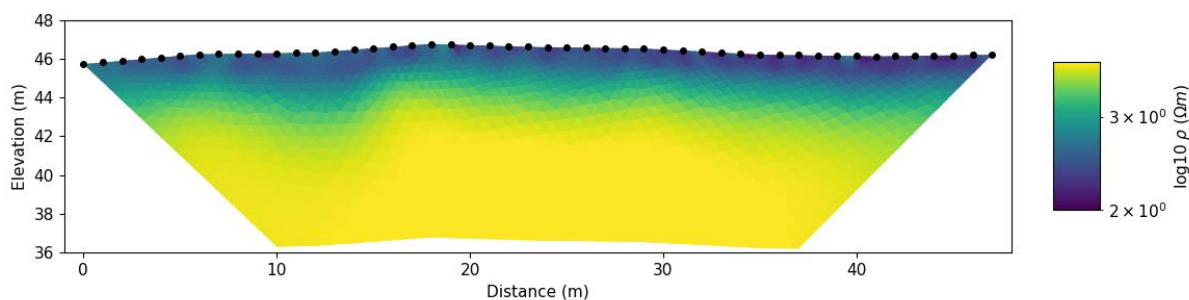
Figure 5: Resistivity model obtained from the inversion of ERT_P1_Par. The acquisition configuration is WS. The minimum and maximum boundaries of the color bar are 100 and 3000 Ωm, respectively.

Another representative example of results is ERT9, since it was acquired with 10 m of electrode spacing and with different quadrupole configurations (DD, WS, WE). The inversion results for the ERT9 are presented in Fig. 6. The general picture presented by the three models is basically the same, but the DD (Fig. 6-top), having a higher lateral sensitivity and data coverage, offers a more resolved picture of the underlying electrical structure. Among the three models, the less informative one seems the WE (Fig. 6-bottom), which is highly resembling the WS model (Fig. 6-center), but with low resolution in terms of spatial data coverage and array characteristics.
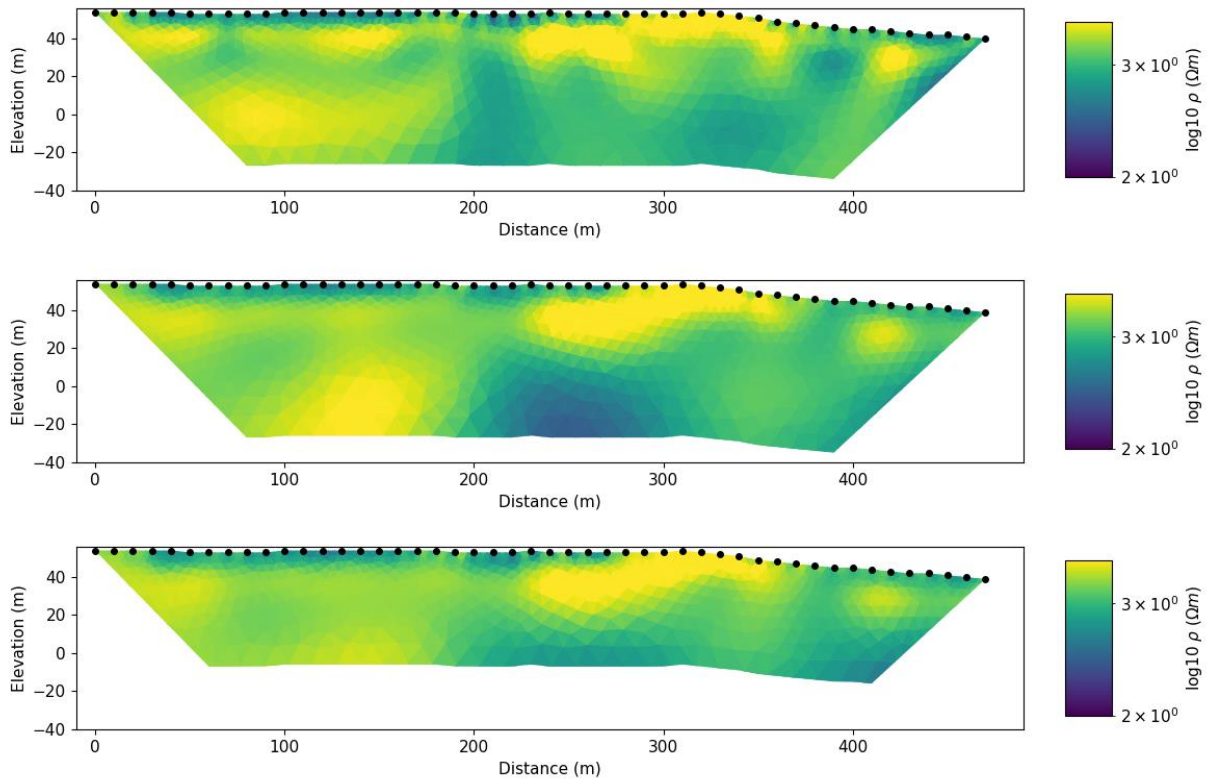
310

Figure 6: Resistivity model obtained from the inversion of ERT9. Different acquisition configurations: top) DD; center) WS; bottom) WE. The minimum and maximum boundaries of the color bar are 100 and 3000 Ωm, respectively.

315   The post-processing analysis of the inversion results was carried out in Matlab® environment, where we imported the ResIPy output (that is, the file "f001_err.dat") to plot the spatial distribution of apparent resistivity (observed and calculated) and the errors. The Matlab script to generate this kind of figure is provided in the repository for reproducibility, in the folder "***ERT/Example results***", under the name "*Post_processing_Matlab.pdf*".

Fig. 7 shows an example of post-processing for ERT_P1_Par (WS configuration). There is no topography in this kind of
320   representation since the vertical axis is a pseudo-depth. The three panels illustrate the pseudo-sections of measured data (top), computed apparent resistivities (center) and the misfit between them (bottom). The pseudo-depth was calculated following Edwards (1977) that is the same approach adopted in ResIPy (Fig. 3). The computed response is the apparent resistivity values that one would obtain performing a measuring operation on a subsoil in which the resistivity is distributed exactly as in the calculated resistivity model as in Fig. 5. The lower the misfit between the observed and calculated data, the
325   more the reliability of the inversion results.
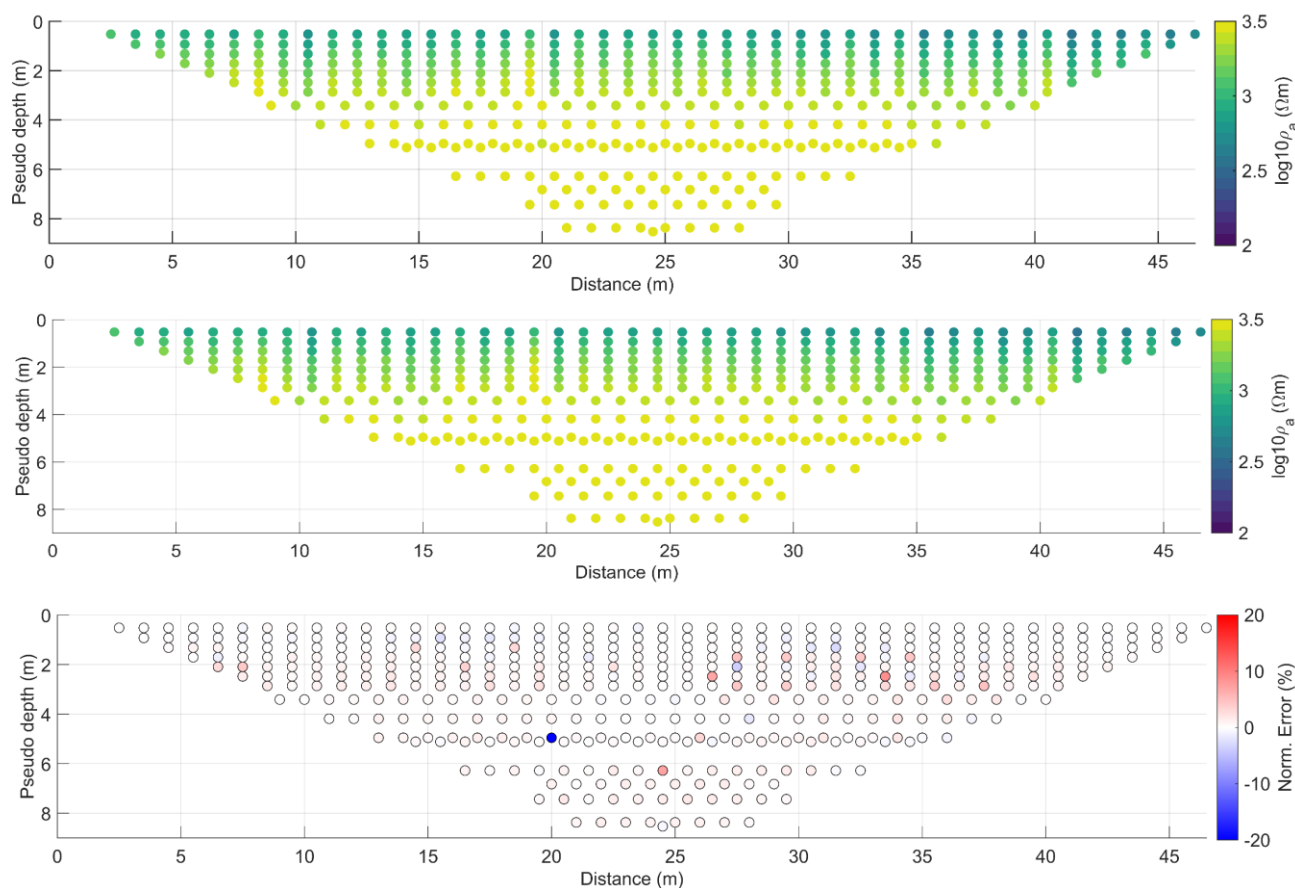
Figure 7: Post-processing analysis of the ResIPy inversion result for ERT_P1_Par, WS configuration: top) observed data (ρ_a);
center) calculated response (ρ_a); bottom) misfit between them, calculated as normalized error in percentage.

5.3 GPR result

To calculate the depth of the reflections, it is necessary to determine the propagation speed of the radar waves in the investigated levels. This is mainly related to the physical–electrical characteristics of the investigated medium. In particular, in a low-loss material, it is inversely proportional to the square root of the dielectric constant (ε_r) and is estimated or calculated through various possibilities of signal analysis or with experimental calibration tests. The data processing enables the conversion of the propagation speed of the radar waves into the subsoil depth. Finally, the digital acquisition allows the representation of the acquired data in 2D-profiles, as can be seen in Fig. 8. It shows GPR_P1_Par, a representative GPR line that is parallel to ERT_P1_Par and acquired with the 400 MHz antenna.

The 2D GPR profiles can be finally filtered and enhanced to detect and locate geological features.
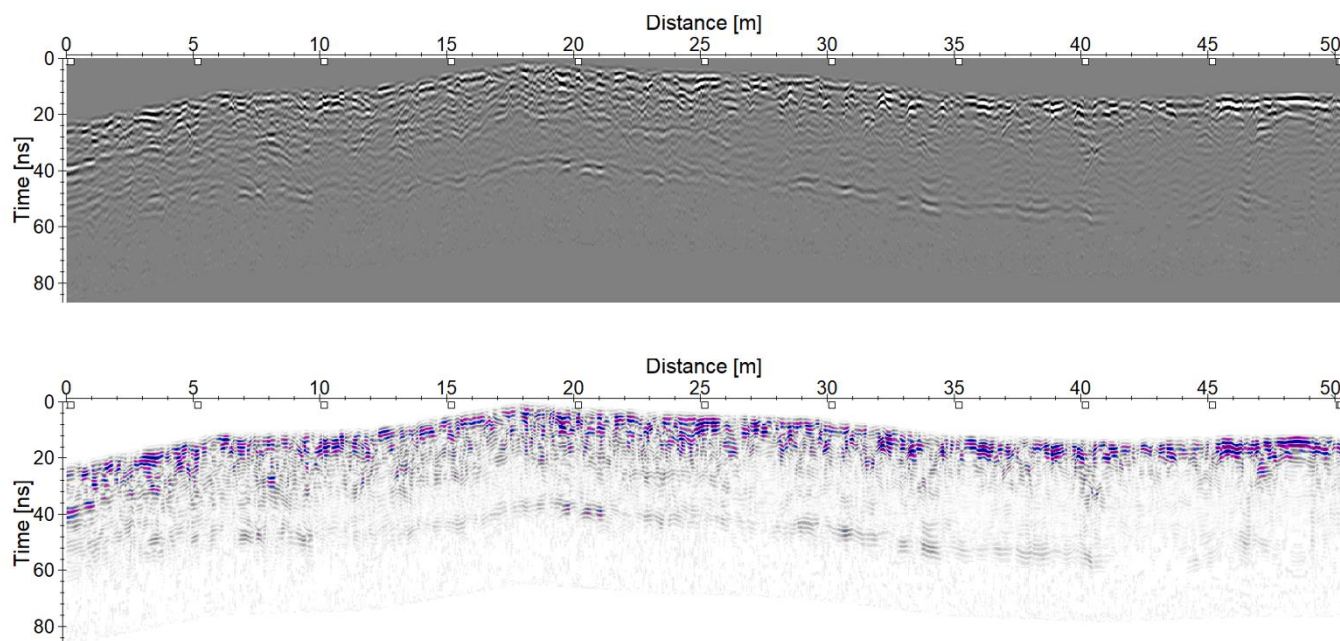
340

Figure 8: Example of a processed 2D radargram for GPR_P1_Par, which is parallel to ERT_P1_Par and was acquired with the 400 MHz antenna. The radargram is shown in two different color scales.

6 Database publication of data and results

This paragraph is mainly dedicated to the readers interested to download and reuse the data. The aim is to provide raw and
345 processed data in formats that are friendly for geophysical software, in order to allow geoscientists to visualize them best, and reprocess them. We also provide the two representative inversion models shown in Figs. 5 and 6 as ready-to-use profiles of electrical resistivity of the subsoil, for scientists interested to directly use the results for multidisciplinary studies, e.g., to produce geologic or hydrogeologic models, and for comparison of different inversion schemes. The coupled data sets of ERT and GPR data along the 9 coincident profiles can also be used to test different joint inversion schemes.

350 **6.1 Repository organization**

The repository is organized in two main folders, as shown in Fig. 9: ***ERT*** and ***GPR*** (the folder names are highlighted in bold italic).

The subfolder ***Data*** in ***ERT*** contains 18 subfolders, one for each deep ERTs (from ***ERT1*** to ***ERT10***), and each shallow ERTs close to the four piezometers (from ***ERT_P1_Par/Ort*** to ***ERT_P4_Par/Ort***). With regards to the latter, the notations "Ort"
355 and "Par" refer to orthogonal and parallel directions with respect to the ERT10 that crosses the piezometers, respectively.

Schematic information about the ERT profiles is shown in Table 1. The scheme of the folder organization is depicted in Fig. 9.

Each of the 18 ERT profile folders contains the following subfolders:

- ***1_Raw_data***: it contains .bin files, as saved by the Syscal Pro georesistivimeter. The .bin files contain the elevation
360   information for each electrode and its relative position in the line. The files do not include the geographical East and North coordinates of the electrodes.

- ***2_Filtered_data_inversion_input***: it contains a .Dat file which is the classical input format for performing the inversion in RES2DINV software, also readable by ResIPy. This folder contains the ResIPy project file (.resipy) with embedded the electrode coordinates, the topography, the mesh created for the inversion, the inversion settings
365   and result. The folder stores a .png image of the pseudosection of the apparent resistivity. For ***DD*** surveys, the evaluation of the reciprocal error was calculated, that is, the difference between resistivity measurements performed on the same quadrupole, but with transmitter and receiver electrodes switched. For ***DD*** surveys there are hence supplementary files: a .csv file ("ErrorData.csv") storing the calculated errors, a .Dat file ("#_rec_err.Dat") that allows the ResIPy inversion to be performed by accounting the reciprocal errors, two figures (.png) that show the
370   resistance error plot and the spatial distribution of the reciprocal errors.

- ***3_Topography***: it contains a .csv file with columns representing the electrode number, East, North and altitude, in Coordinate Reference System (CRS) WGS84, projection UTM, zone 33N (EPSG 32633). The East and North coordinates were collected during geophysical acquisition thanks to GPS measurements. We considered inadequate the accuracy of the altitude measurements by GPS, so the surface topography was retrieved from a 5-m digital
375   elevation model (DEM) of the area openly provided by the Norwegian Polar Institute (©Norwegian Polar Institute, 2014, https://geodata.npolar.no/).

Each subfolder is organized according to the **Q*uadrupole configuration***, that is, in ***WS*** (Wenner - Schlumberger), ***DD*** (Dipole - Dipole) and, if measured, ***WE*** (Wenner).

The repository stores some representative results of ERT 2D inversion for the two profiles shown in the Section 5.1 (i.e.,
380 ERT_P1_Par and ERT9). Their location in the repository is in folder ***Example results*** in ***ERT***, where for each profile there is a folder ***Inversion_model*** (see Fig.9). It contains, for each **Q*uadrupole configuration***, the result of the inversion, that is, the sections of electrical resistivity of the subsoil. This folder appears for the lines shown in Figs. 5 and 6 (i.e., ERT_P1_Par and ERT9). The 2D resistivity models are provided as .png images for fast visualization (e.g., "Model.png", "Misfit.png", "NormErrors.png"), and .vtk files to allow further visualization processing in software like Paraview (Hansen and Johnson,
385 2005). Other relevant files in this folder are the "3plot.tif" file, which shows pseudosections of the measured and computed apparent resistivity and their difference (as in Fig. 7), and the mesh files .geo and .msh, readable by Gmsh software (Geuzaine and Remacle, 2009). The remaining files (e.g., "electrodes.dat", "protocol.dat", "R2.out") are automatically generated and saved by ResIPy and have the same name of the corresponding files saved by the freeware package R2 (Binley, 2023), whose manual is free to access.

390   The ***Data*** folder in ***GPR*** folder contains 10 subfolders (***Profile Name*** in Fig. 9) for each transect, 8 of which are coincident with the 8 shallow ERTs described above, and the other two are on the same path of ERT10 (i.e., ***GPR_Long_40MHz*** and ***GPR_Long_400MHz***). The eight short GPR profiles were measured with a 400 MHz antenna and centered in the four I2F piezometers. Schematic information about the GPR profiles is shown in Table 2. Each folder of GPR profiles contains four files (see Fig. 9):

395   -   the original file of raw data in .DZT (Radan) format;

         -    the file of raw data in SEGY format (.SGY);

         -    the marker file (.MAR) that stores the number of the trace (first column) and the distance along the profile (second column).

         -    the text file (.txt) for the topography, which contains the distance along the profile (first column), a second

400   column of zeros and the corresponding elevation (third column).

An example of processed data is provided for profile GPR_P1_Par (Fig. 8), inside folder ***Example result*** in ***GPR***. The data were processed according to the workflow explained in Fig. 4 and saved in Reflexw format and in SEGY format. The files following the Reflexw format are named "GPR_P1_Par_processed.04R" and "GPR_P1_Par_processed.04T", while the remaining file is "GPR_P1_Par_processed.SGY". The processed files in Reflexw and SEGY format have topographic

405 correction. The image file is provided for fast visualization.
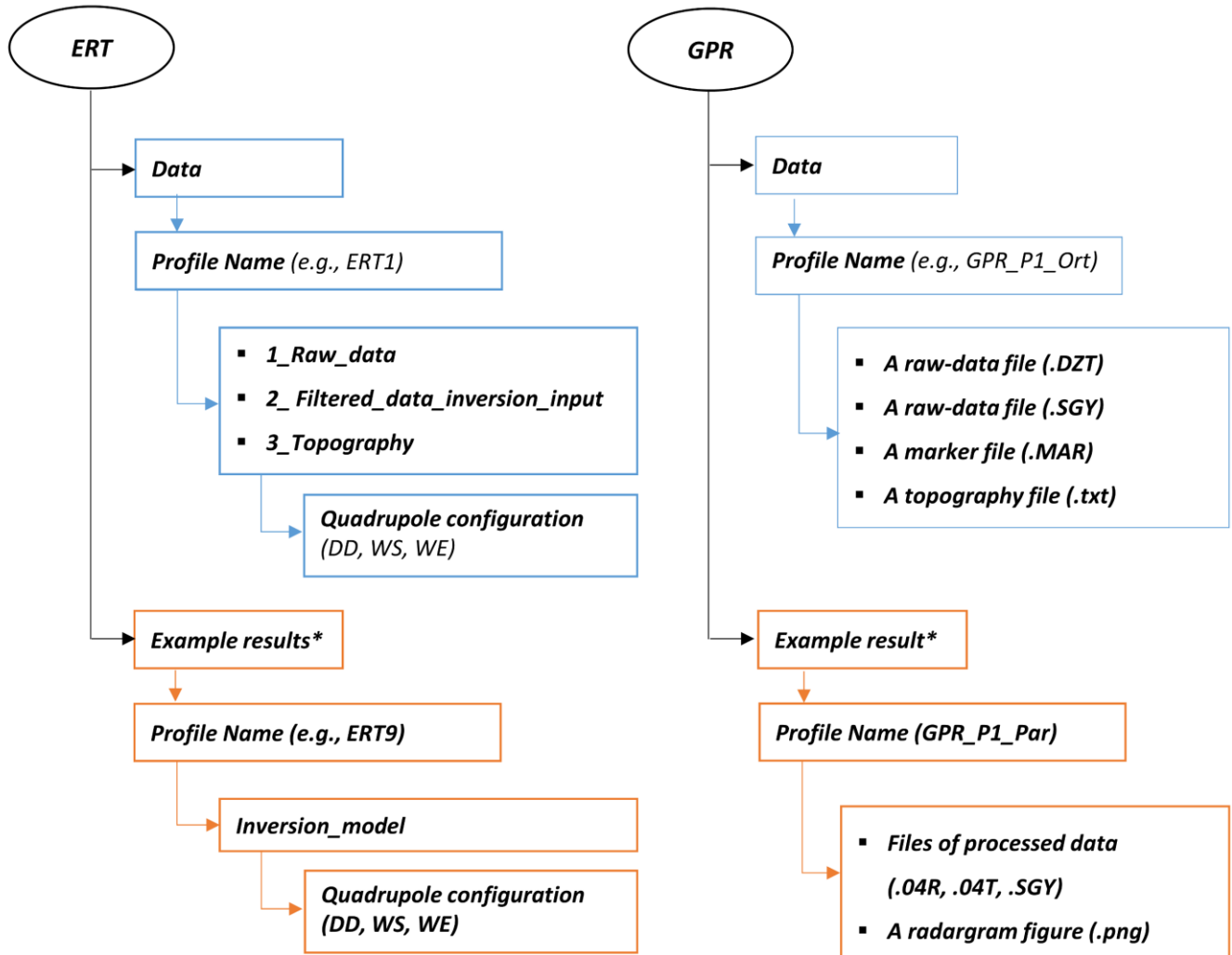
Figure 9: the workflow of the repository of ERT and GPR data acquired in Ny-Ålesund.

6.2 Specifications of data file

In this section, the main file types used for sharing the ERT and GPR data are described.

410 **6.2.1. ERT**

The apparent resistivity values are given in a text file with .DAT extension, according to the RES2DINV format (Loke, 2004). The data can be edited using any general-purpose text editor to check and manually modify the data file. The data are arranged in an ASCII delimited manner where a comma or blank space or LF/CR is used to separate different numerical data

items. The data format used here is a general array format, to include non-conventional arrays of any configuration. The data
415 file is organized in three different slots: the headers, the apparent resistivity section, and the topographical section. The
headers include the flag of the configuration array, the number of apparent resistivity data and other information on the
transect. The data are organized in nine columns: the x and z coordinates of the four electrodes for each sequence and the
column of apparent resistivity (in Ωm). Additional information and details about how the data files are structured are
reported in the RES2DINV Manual and Loke's Course Notes. A description of the different array types is given in the free
420 tutorial notes on electrical imaging (Loke, 2004). The topography data are below the section with the apparent resistivity
values, separated by them by some specific flags. The first item is a flag to indicate whether the file contains topography
data. If there is no topography data, its value is 0. We entered 1 or 2 to indicate that topographical data is present. In most
transects, the distances of the points are taken along the ground surface; in this case, the value of 2 for the topography data
flag is considered. This is followed by the number of topographical data points. At the end, some 0 flags are included.

425 **6.2.2 GPR**

The GPR data are available in SEG-Y (Hagelund and Levin, 2017) after being converted from the original files in
proprietary RADAN format (with extension .DZT). The SEG-Y is an open standard format developed by the Society of
Exploration Geophysicists in 1975, nevertheless, it remains the preferred preservation file format for GPR data. The files
have been post-processed according to the workflow provided in Section 4 and then converted to SEG-Y format. The
430 conversion and post-processing were performed using Reflexw Software (Sandmeier, 2021). The conversion was performed
following these settings: exporting format SEGY-DOS, scaling factor for coordinates equal to 1, and checking the output
parameters "segy_ibm_format" and "ps timeincr". This SEG-Y format provides a file with IBM 32-bit floating-point
numbers. We tested the files with Reflexw and GPR-Viewer to validate them before the distribution.

7 Data availability

435 Data described in this manuscript can be accessed at the repository under data doi:
https://zenodo.org/doi/10.5281/zenodo.10260056 (Pace et al., 2023).

8 Conclusions

This paper set out to share a data set of geophysical survey, performed in the summer of 2022 in the Svalbard Archipelago,
near the Ny-Ålesund village. The survey was undertaken to provide new insight into the hydrogeological characterization of
440 the area.
We have described the acquisition settings of ERT and GPR data in such an extreme environment, that of remote High
Arctic tundra. The details of all the acquired profiles were listed. Then, the methods adopted for quality control and

processing were illustrated. Some representative examples of processed data and inversion results were shown in this manuscript, and together with the whole data set, were organized to be shared in a public repository.

445 The data set has been carefully uploaded to the repository using a common and standard geophysical format for an easy-to-use processing with commercial and not commercial software. All the transects are completed with the topographical information and have been tested by checking their integrity and functionality. The repository is available under data doi (Pace et al.,2023, https://zenodo.org/doi/10.5281/zenodo.10260056).

The public availability of this repository is of major relevance because to the authors' knowledge no data set of near-surface
450 geophysical acquisitions, such as the one presented here, has been published, even though the Ny-Ålesund represents the northernmost popular scientific center in the High Arctic.

The data have been collected mostly for 2D interpretation even if an attempt of pseudo-3D data processing could be possible, especially in the piezometer area. In this area, we also share the data set of GPR data that could be useful for data integration or joint inversion. This would be a fruitful area for future work.

455 Our data set could offer a good opportunity for geophysicists to develop new methodologies for interpreting geophysical data in the Arctic environment and for geoscientists, involved in studying the region, to corroborate their assumptions about the geological and hydrogeological settings of the area.

Future work will investigate the interpretation of the geophysical models by means of hydrogeological and geological information and in collaboration with other partners of the I2F project.

460 The data set is shared with the scientific community for all the possible purposes. Future users are kindly asked to cite the present paper when using the data set.

Glossary

DD: Dipole-Dipole Array configuration for ERT data

ERT: Electrical Resistivity Tomography

465 GPR: Ground Penetrating Radar

GPS: Global Positioning System

I2F: ICEtoFLUX project

MT: Magnetotelluric method

UTM: Universal Transverse Mercator

470 WS: Wenner-Schlumberger Array configuration for ERT data

WE: Wenner Array configuration for ERT data

Author contribution

Data curation: FP, AV, AG, GR, AS, LC;

data acquisition and fieldwork: FP, AV, AG, GR, AS, LC, IB;

475 methodology and modeling: FP, AV, AG, GR, AS, LC;

software: FP, AV, AG, GR, AS, LC;

supervision: AG, AS, MD;

visualization: FP, AV, GR, AS, LC;

writing – original draft: FP, AV, AG, GR, AS, LC;

480 writing – review & editing: all.

Competing interests

The authors declare that they have no conflict of interest.

Acknowledgements

The authors would like to thank Diego Franco (Politecnico di Torino) for his help in setting up the instrumentation before
485 and after the Arctic expedition. Further thanks go to the station leaders of the Italian Arctic Station Marco Casula and
Ombretta Dell'Acqua for their support during the fieldwork in summer 2022. We would also like to show our gratitude to
the polar bears of the Svalbard Islands that did not eat us, this time.

Financial support

The research project ICEtoFLUX ("HydrologIcal changes in ArctiC Environments and water-driven biogeochemical
490 FLUXes") was financed by Arctic Research Program MUR-PRA 2021-0027 (RIS 11795). The research activity of F. Pace
was carried out within the Ministerial Decree no. 1062/2021 and received funding from the FSE REACT-EU - PON Ricerca
e Innovazione 2014-2020.

References

Beka, T. I., Senger, K., Autio, U. A., Smirnov, M., and Birkelund, Y.: Integrated electromagnetic data investigation of a
495 Mesozoic CO2 storage target reservoir-cap-rock succession, Svalbard, Journal of Applied Geophysics, 136, 417–430,
https://doi.org/10.1016/j.jappgeo.2016.11.021, 2017.

Binley, A.: R2 (Version 4.10), 2023.

Blanchy, G., Saneiyan, S., Boyd, J., McLachlan, P., and Binley, A.: ResIPy, an intuitive open source software for complex geoelectrical inversion/modeling, Computers & Geosciences, 137, 104423, https://doi.org/10.1016/j.cageo.2020.104423, 2020.

Boike, J., Roth, K., and Ippisch, O.: Seasonal snow cover on frozen ground: Energy balance calculations of a permafrost site near Ny-Ålesund, Spitsbergen, J. Geophys. Res., 108, https://doi.org/10.1029/2001JD000939, 2003.

Boike, J., Juszak, I., Lange, S., Chadburn, S., Burke, E., Overduin, P. P., Roth, K., Ippisch, O., Bornemann, N., Stern, L., Gouttevin, I., Hauber, E., and Westermann, S.: A 20-year record (1998–2017) of permafrost, active layer and meteorological conditions at a high Arctic permafrost research site (Bayelva, Spitsbergen), Earth Syst. Sci. Data, 10, 355–390, https://doi.org/10.5194/essd-10-355-2018, 2018.

Booij, M., Leijnse, A., Haldorsen, S., Heim, M., and Rueslåtten, H.: Subpermafrost Groundwater Modelling in Ny-Ålesund, Svalbard, Hydrology Research, 29, 385–396, https://doi.org/10.2166/nh.1998.0030, 1998.

Byun, Y.-H., Yoon, H.-K., Kim, Y. S., Hong, S. S., and Lee, J.-S.: Active layer characterization by instrumented dynamic cone penetrometer in Ny-Alesund, Svalbard, Cold Regions Science and Technology, 104–105, 45–53, https://doi.org/10.1016/j.coldregions.2014.04.003, 2014.

Chave, A. D., Jones, A. G., Mackie, R., and Rodi, W.: The Magnetotelluric Method: Theory and Practice, Cambridge University Press, Cambridge, https://doi.org/10.1017/CBO9781139020138, 2012.

Dallmann, W. K. (Ed.): Geoscience atlas of Svalbard, Norsk polarinstitutt, Tromsø, 292 pp., 2015.

Doveri, M., Lelli, M., Baneschi, I., Raco, B., Trifirò, S., Calvi, E., and Provenzale, A.: Glacial drainges and trasfer of freshwater to the Arctic Ocean in Kongsfjorden (Svalbard), 16518, 2019.

Doyoro, Y. G., Chang, P.-Y., Puntu, J. M., Lin, D.-J., Van Huu, T., Rahmalia, D. A., and Shie, M.-S.: A review of open software resources in python for electrical resistivity modelling, Geosci. Lett., 9(1), 1–16, https://doi.org/10.1186/s40562-022-00214-1, 2022.

Edwards, L. S.: A modified pseudosection for resistivity and IP, GEOPHYSICS, 42, 1020–1036, https://doi.org/10.1190/1.1440762, 1977.

Geuzaine, C. and Remacle, J.-F.: Gmsh: A 3-D finite element mesh generator with built-in pre- and post-processing facilities: THE GMSH PAPER, Int. J. Numer. Meth. Engng., 79, 1309–1331, https://doi.org/10.1002/nme.2579, 2009.

Gevers, M., David, D. T., Thakur, R. C., Hübner, C., and Jania, J.: SESS report 2022, Svalbard Integrated Arctic Earth Observing System, Longyearbyen, 2023.

Hagelund, R. and Levin, S. A.: SEG-Y_r2.0: SEG-Y revision 2.0 Data Exchange format, SEG Technical Standards Committee, 1–151, https://doi.org/10.1190/tle36050449.1, 2017.

Haldorsen, S. and Heim, M.: An arctic groundwater system and its dependence upon climatic change: an example from Svalbard, Permafrost and Periglacial Processes, 10, 137–149, https://doi.org/10.1002/(SICI)1099-1530(199904/06)10:2<137::AID-PPP316>3.0.CO;2-%23, 1999.

Hansen, C. D. and Johnson, C. R. (Eds.): The visualization handbook, Elsevier-Butterworth Heinemann, Amsterdam; Boston, 962 pp., 2005.

Hauck, C. and Kneisel, C. (Eds.): Applied Geophysics in Periglacial Environments, 1st ed., Cambridge University Press, https://doi.org/10.1017/CBO9780511535628, 2008.

535 Hoel, A.: The coal deposits and coal mining of Svalbard (Spitsbergen and Bear Island), Oslo, 92 pp., 1925.

Hornum, M. T., Betlem, P., and Hodson, A.: Groundwater Flow Through Continuous Permafrost Along Geological Boundary Revealed by Electrical Resistivity Tomography, Geophysical Research Letters, 48, e2021GL092757, https://doi.org/10.1029/2021GL092757, 2021.

Horota, R. K., Senger, K., Rodes, N., Betlem, P., Smyrak-Sikora, A., Jonassen, M. O., Kramer, D., and Braathen, A.: West
540 Spitsbergen fold and thrust belt: A digital educational data package for teaching structural geology, Journal of Structural Geology, 167, 104781, https://doi.org/10.1016/j.jsg.2022.104781, 2023.

Jol, H. M.: Ground Penetrating Radar Theory and Applications, Elsevier, https://doi.org/10.1016/B978-0-444-53348-7.X0001-4, 2009.

Kasprzak, M., Strzelecki, M. C., Traczyk, A., Kondracka, M., Lim, M., and Migała, K.: On the potential for a bottom active
545 layer below coastal permafrost: the impact of seawater on permafrost degradation imaged by electrical resistivity tomography (Hornsund, SW Spitsbergen), Geomorphology, 293, 347–359, https://doi.org/10.1016/j.geomorph.2016.06.013, 2017.

Keating, K., Binley, A., Bense, V., Van Dam, R. L., and Christiansen, H. H.: Combined Geophysical Measurements Provide Evidence for Unfrozen Water in Permafrost in the Adventdalen Valley in Svalbard, Geophysical Research Letters, 45, 7606–
550 7614, https://doi.org/10.1029/2017GL076508, 2018.

Killingtveit, Å., Pettersson, L.-E., and Sand, K.: Water balance investigations in Svalbard, Polar Research, 22, 161–174, https://doi.org/10.1111/j.1751-8369.2003.tb00105.x, 2003.

KODAMA, Y., Yukari, T., Hironori, N., and Okitsugu, W.: HYDROLOGICAL OBSERVATIONS IN BREGGER GLACIER BASIN, SPITSBERGEN : DISCHARGE, TEMPERATURE AND ELECTRIC CONDUCTIVITY,
555 https://doi.org/10.15094/00003878, September 1995.

Köhler, A., Nuth, C., Schweitzer, J., Weidle, C., and Gibbons, S. J.: Regional passive seismic monitoring reveals dynamic glacier activity on Spitsbergen, Svalbard, Polar Research, 34, 26178, https://doi.org/10.3402/polar.v34.26178, 2015.

Kohler, J., Moore, J. C., and Isaksson, E.: Comparison of modelled and observed responses of a glacier snowpack to ground-penetrating radar, Ann. Glaciol., 37, 293–297, https://doi.org/10.3189/172756403781815528, 2003.

560 Koster, B. and Kruse, F.: The use of ground penetrating radar (GPR) in the investigation of historical quarry abandonment in Svalbard, Polar Record, 52, 330–344, https://doi.org/10.1017/S0032247415000844, 2016.

Kumari, S., Pandit, A., Patel, L., Ramsankaran, R., Sharma, P., and Ramanathan, A. L.: Modelling ice thickness and storage volume of svalbard glaciers monitored through Indian Arctic Programme, Polar Science, 30, 100741, https://doi.org/10.1016/j.polar.2021.100741, 2021.

565 Kuschel, E., Eppinger, S., Bernard, E., Tolle, F., Prokop, A., Friedt, J.-M., and Zangerl, C.: Landslide monitoring using multi-temporal terrestrial laser scanning (TLS) and electrical resistivity tomography (ERT) in the high Arctic, Ny-Ålesund, Geophysical Research Abstracts, 21, 13733, 2019.

Lee, J.-S., Hong, W.-T., Park, K., Hong, S., Lee, S.-H., and Byun, Y.-H.: Evaluation of Water Content in an Active Layer Using Penetration-Type Time Domain Reflectometry, Applied Sciences, 8, 935, https://doi.org/10.3390/app8060935, 2018.

570 Lindbäck, K., Kohler, J., Pettersson, R., Nuth, C., Langley, K., Messerli, A., Vallot, D., Matsuoka, K., and Brandt, O.: Subglacial topography, ice thickness, and bathymetry of Kongsfjorden, northwestern Svalbard, Earth Syst. Sci. Data, 10, 1769–1781, https://doi.org/10.5194/essd-10-1769-2018, 2018.

Loke, M. H.: Tutorial: 2-D and 3-D electrical imaging surveys, 2004.

Loke, M. H., Chambers, J. E., Rucker, D. F., Kuras, O., and Wilkinson, P. B.: Recent developments in the direct-current 575 geoelectrical imaging method, Journal of Applied Geophysics, 95, 135–156, https://doi.org/10.1016/j.jappgeo.2013.02.017, 2013.

Martorana, R., Capizzi, P., D'Alessandro, A., and Luzio, D.: Comparison of different sets of array configurations for multichannel 2D ERT acquisition, Journal of Applied Geophysics, 137, 34–48, https://doi.org/10.1016/j.jappgeo.2016.12.012, 2017.

580 Mémin, A., Spada, G., Boy, J.-. P., Rogister, Y., and Hinderer, J.: Decadal geodetic variations in Ny-Ålesund (Svalbard): role of past and present ice-mass changes, Geophysical Journal International, 198, 285–297, https://doi.org/10.1093/gji/ggu134, 2014.

Norwegian Polar Institute: Terrengmodell Svalbard (S0 Terrengmodell) [Data set]. Norwegian Polar Institute., https://doi.org/10.21334/npolar.2014.dce53a47, 2014.

585 Orvin, A. K.: Geology of the King's Bay Region, Spitsbergen. By A. K. Orvin. *Skrifter om Svalbard og Ishavet* . Nr. 57. pp. 195, with 3 plates, 4 maps, and 52 text-figures. Oslo: Jacob Dybwad, 1934, Geol. Mag., 57, 195, https://doi.org/10.1017/S0016756800093328, 1934.

Pace, F., Vergnano, A., Godio, A., Romano, G., Capozzoli, L., Baneschi, I., Doveri, M., and Santilano, A.: A new repository of electrical resistivity tomography and ground penetrating radar data from summer 2022 near Ny-Ålesund, Svalbard, 590 Zenodo [data set] (0), https://zenodo.org/doi/10.5281/zenodo.10260056, 2023.

Paglia, E.: A higher level of civilisation? The transformation of Ny-Ålesund from Arctic coalmining settlement in Svalbard to global environmental knowledge center at 79° North, Polar Record, 56, e15, https://doi.org/10.1017/S0032247419000603, 2020.

Park, K., Kim, K., Kim, K., and Hong, W.-T.: Characterization of active layer at different degrees of patterned ground 595 development using electrical resistivity tomography survey, Cold Regions Science and Technology, 208, 103734, https://doi.org/10.1016/j.coldregions.2022.103734, 2023.

Pedersen, Å. Ø., Convey, P., Newsham, K. K., Mosbacher, J. B., Fuglei, E., Ravolainen, V., Hansen, B. B., Jensen, T. C., Augusti, A., Biersma, E. M., Cooper, E. J., Coulson, S. J., Gabrielsen, G. W., Gallet, J. C., Karsten, U., Kristiansen, S. M., Svenning, M. M., Tveit, A. T., Uchida, M., Baneschi, I., Calizza, E., Cannone, N., De Goede, E. M., Doveri, M., Elster, J., 600 Giamberini, M. S., Hayashi, K., Lang, S. I., Lee, Y. K., Nakatsubo, T., Pasquali, V., Paulsen, I. M. G., Pedersen, C., Peng, F., Provenzale, A., Pushkareva, E., Sandström, C. A. M., Sklet, V., Stach, A., Tojo, M., Tytgat, B., Tømmervik, H., Velazquez, D., Verleyen, E., Welker, J. M., Yao, Y.-F., and Loonen, M. J. J. E.: Five decades of terrestrial and freshwater research at Ny-Ålesund, Svalbard, Polar Research, 41, https://doi.org/10.33265/polar.v41.6310, 2022.

Pramanik, A., Van Pelt, W., Kohler, J., and Schuler, T. V.: Simulating climatic mass balance, seasonal snow development and associated freshwater runoff in the Kongsfjord basin, Svalbard (1980–2016), J. Glaciol., 64, 943–956, https://doi.org/10.1017/jog.2018.80, 2018.

Repp, K.: The Hydrology of Bayelva, Spitsbergen, Hydrology Research, 19, 259–268, https://doi.org/10.2166/nh.1988.0018, 1988.

Rossi, M., Dal Cin, M., Picotti, S., Gei, D., Isaev, V. S., Pogorelov, A. V., Gorshkov, E. I., Sergeev, D. O., Kotov, P. I., Giorgi, M., and Rainone, M. L.: Active Layer and Permafrost Investigations Using Geophysical and Geocryological Methods—A Case Study of the Khanovey Area, Near Vorkuta, in the NE European Russian Arctic, Front. Earth Sci., 10, 910078, https://doi.org/10.3389/feart.2022.910078, 2022.

Saintenoy, A., Friedt, J.-M., Tolle, F., Bernard, E., Laffly, D., Marlin, C., and Griselin, M.: High density coverage investigation of The Austre LovénBreen (Svalbard) using Ground Penetrating Radar, 2011 6th International Workshop on Advanced Ground Penetrating Radar (IWAGPR 2011), Aachen, Germany, 1–4, https://doi.org/10.1109/IWAGPR.2011.5963894, 2011.

Saintenoy, A., Friedt, J. -M., Booth, A. D., Tolle, F., Bernard, E., Laffly, D., Marlin, C., and Griselin, M.: Deriving ice thickness, glacier volume and bedrock morphology of Austre Lovénbreen (Svalbard) using GPR, Near Surface Geophysics, 11, 253–262, https://doi.org/10.3997/1873-0604.2012040, 2013.

Sandmeier, K. J.: Reflexw Version 9.5 Windows™ XP/7/8/10-program for the processing of seismic, acoustic or electromagnetic reflection, refraction and transmission data, Sandmeyer geophysical research, 2021.

Schannwell, C., Murray, T., Kulessa, B., Gusmeroli, A., Saintenoy, A., and Jansson, P.: An automatic approach to delineate the cold–temperate transition surface with ground-penetrating radar on polythermal glaciers, Ann. Glaciol., 55, 89–96, https://doi.org/10.3189/2014AoG67A102, 2014.

Schwamborn, G., Heinzel, J., Schirrmeister, L., and Boike, J.: Verifying georadar records from permafrost in the Ny-Ålesund area using core data and wavelet modelling, AWIPEV - Workshop, Joint French-German Collaborations for science in Svalbard, Strassbourg, France, 2005.

Schwamborn, G., Heinzel, J., and Schirrmeister, L.: Internal characteristics of ice-marginal sediments deduced from georadar profiling and sediment properties (Brøgger Peninsula, Svalbard), Geomorphology, 95, 74–83, https://doi.org/10.1016/j.geomorph.2006.07.032, 2008.

Soldovieri, F., Prisco, G., and Hamran, S.-E.: A preparatory study on subsurface exploration on Mars using GPR and microwave tomography, Planetary and Space Science, 57, 1076–1084, https://doi.org/10.1016/j.pss.2008.11.014, 2009.

Son, D. and Lee, E. J.: Soil Microbial Communities Associated with Three Arctic Plants in Different Local Environments in Ny–Ålesund, Svalbard, J. Microbiol. Biotechnol., 32, 1275–1283, https://doi.org/10.4014/jmb.2208.08009, 2022.

Svendsen, H., Beszczynska-Møller, A., Hagen, J. O., Lefauconnier, B., Tverberg, V., Gerland, S., Børre Ørbæk, J., Bischof, K., Papucci, C., Zajaczkowski, M., Azzolini, R., Bruland, O., and Wiencke, C.: The physical environment of Kongsfjorden–Krossfjorden, an Arctic fjord system in Svalbard, Polar Research, 21, 133–166, https://doi.org/10.3402/polar.v21i1.6479, 2002.

Tolle, F., Bernard, E., Friedt, J. M., Saintenoy, A., Marlin, C., and Griselin, M.: Data issues in a moving environment: remote and in situ tools to monitor glacier dynamics and their hydrological consequences in the Austre Lovènbreen basin, 10th Ny-Ålesund Seminar, 2011.

1["